# Modelling and mechanical design of a flexible tube-guided SMA actuator

Liu, Qiang; Ghodrat, Sepideh; Jansen, Kaspar M.B.

**DOI**
10.1016/j.matdes.2022.110571

**Publication date**
2022

**Document Version**
Final published version

**Published in**
Materials and Design

Materials & Design 216 (2022) 110571

Contents lists available at ScienceDirect

Materials & Design

journal homepage: www.elsevier.com/locate/matdes

# Modelling and mechanical design of a flexible tube-guided SMA actuator

Qiang Liu *, Sepideh Ghodrat *, Kaspar M.B. Jansen

*Emerging Materials Laboratory, Department of Sustainable Design Engineering, Delft University of Technology (TU Delft), Landbergstraat 15, Delft, 2628 CE, the Netherlands*

## HIGHLIGHTS

- An accurate phenomenological model of the tube-guided shape memory alloy (SMA) actuator is proposed.
- The model describes how the actuation stroke changes under the influence of parameters such as stress, temperature and time.
- The model can support designers and engineers to efficiently adopt the system without having to work with constitutive material models.

## GRAPHICAL ABSTRACT

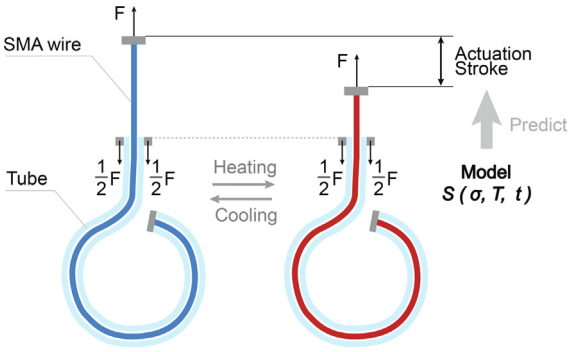


## ARTICLE INFO

*Article history:*
Received 31 January 2022
Revised 1 March 2022
Accepted 18 March 2022
Available online 21 March 2022

*Keywords:*
Tube-guided SMA actuators
Phenomenological model
Wearable actuators
Soft robotics

## ABSTRACT

Shape memory alloy (SMA) wires are excellent candidates for wearable actuators since they are thin, low weight and have a high actuation force. The main drawbacks are that the wire should be kept straight and needs to be relatively long to enable a large enough actuation stroke. Embedding the SMA wire in a flexible tube largely enhances its applicability since then the counter forces are transferred by the tube material and the tube can be rolled up or attached to flexible surfaces or clothing layers. The performance of such tube-guided SMA actuators is, however, more complicated since it not only depends on the SMA behaviour but also on the tube materials and the actuator construction.

In this research, a simple end-state model for a tube-guided SMA actuator system is proposed. We measure and model both the SMA and tube material properties, including tube creep effects, and derive an approximate prediction for the actuator stroke. Validation experiments showed that the predicted stroke during the second heating and cooling experiments agreed well with the measurements and that the average deviation is 9.6%, even though the deviation is much larger (27.3%) for the maximum applied force.



## 1. Introduction

Shape memory materials (SMM), including shape memory alloy, shape memory polymer, shape memory ceramic, etc., are smart materials with the ability to return to a reference state after an applied deformation. Therefore, they are useful as actuators in practical applications. Common stimuli can be temperature, light intensity, stress, hydrogen potential, electric or magnetic fields [1]. The most commonly used SMM is shape memory alloy (SMA), among which the Ni-Ti (nitinol), Ni-Ti-Cu, Cu-Zn are commercially the most popular. Nitinol has many advantages, and its reliability and low-cost are perhaps the most prominent [1]. In addition, the transformation temperature of the nitinol ranges widely from −200℃ to 200℃ [2]. The nitinol wires used within the specification limits can exhibit repeatable motion for millions of cycles [3].

* Corresponding authors.
*E-mail addresses:* q.liu-6@tudelft.nl (Q. Liu), S.Ghodrat@tudelft.nl (S. Ghodrat).

https://doi.org/10.1016/j.matdes.2022.110571
0264-1275/

In the field of wearable industry, *"Skin+"* [4], the miniature haptic ring [5], and *"ShareHaptics"* [6] are hand devices to improve immersive experiences. Owing to SMA's high strength and ductility, it also shows great potential in smart garments. For instance, compression garment space suit made by SMA knitted actuators can support astronauts' cardiovascular system upon reintroduction to gravitational forces [7]. The *"Hugging Vest"* enables parents or occupational therapists to give comforting "hugs" to children from anywhere in the world [8]. Moreover, SMA shows excellent Magnetic Resonance Imaging (MRI) compatibility and corrosion resistance, which makes it particularly suitable to develop medical rehabilitation or assisting products [9] for people with disabilities. For example, smart nitinol stents have been designed and widely used for improving blood flow [10]. SMA also has a broad application prospect in automotive (e.g. door and locking mechanism, sunroof) and aerospace industries (e.g. wing morphing) [11–13].

The use of shape memory alloy has shown a large growth in the past decade. It is projected that the SMA market will reach 18.97 billion dollars by 2022 [14]. However, as yet, SMA is still insufficiently commercialized. To popularize the SMA applications, there remain many challenges, one of which is the gap between the knowledge of shape memory materials and design. Datasheets are often not complete and are not based on the full understanding of these materials, e.g. many properties are missing. Hence, in most situations, datasheets are not enough to describe performances of an SMA in a specific device. Compared with conventional materials, the constitutive behaviour of shape memory alloys is complicated, as their crystal structures can deform depending on temperature, stress and strain. For designers, it is of crucial importance to be aware of the SMA fundamental working principles.

There have been many models studying the SMA behavior on different levels. For example, based on Tanaka *et al.*'s study [15], Brinson *et al.* used cosine functions to describe the transformation kinetic equations which relate the martensite fraction to the stress and temperature [16]. With several input parameters including transformation stress, transformation temperatures, the maximum recoverable strain, Young's moduli of martensite and austenite, Clausius-Clapeyron constants, and coefficient of thermal expansion, it is possible to calculate the transformation strain of the SMA. Brinson's model succeeds in predicting the SMA's behaviour, and some follow-up reports also embedded Brinson's approach in their models. For instance, Ikuta, *et al.* presented a model based on sigmoid functions [17]. However, in many cases detailed constitutive models might be less practical, as such models try to describe as accurate as possible the relation between the phase transition state temperature, stress and strain, involving thermodynamics of nucleation, growth or interface friction at a molecular level [18]. Alternatively, when designing constructions with SMA actuators, it is often desirable to have simplified models that relate the desired actuation force and displacement that are of relevance to choose actuator parameters (e.g. wire length, or thickness) and can thus be referred to as end-state models.

Both constitutive models and end-state models to some extent can help designers understand fundamental working principles of the SMA. Nevertheless, in practical applications, the SMA generally cannot be used alone in an actuator system. Pre-stretched SMA wires contract when heated above their activation temperatures. During the contraction, they can exert a high actuation force. After cooling down, however, the SMA wires remain in the extended state, as the contraction effect of the wire is not reversible. To make the system function dynamically, it should include passive structural members such as counter weights, additional antagonist SMA wires or bias springs, which are required for resetting the SMA back to its original state. Such SMA-actuator systems are well adopted and many researchers have already developed relevant models for different active systems [2,19].

In this article, a tube-guided SMA actuator is studied. As shown in Fig. 1, a SMA wire threads through a tube, and one end of the wire is fixed with the tube end at *C*. The function of the tube is to transfer the actuator load from the wire end *C* to the tube end *B* while still allowing shape flexibility. The maximum stroke over the actuator is then not 4% of *AB*, but 4% over the full SMA wire length *AC*, even if the tube is not straight but e.g. rolled up. Ideally, the tube should be bendable but stiff in compression. Such configuration has been used in smart garments [20], soft wearable robots [21] as well as rehabilitation devices [22]. The tube-guided SMA actuator is flexible in bending and can provide thermal insulation during actuation of the SMA. When the SMA wire is activated, it contracts within the tube and does not require bearings to support the SMA wire [23]. These advantages also make it a good choice as an actuator for smart textiles.

Tube-guided SMA actuator systems have been studied in literature before. For example, Helps *et al.* found that the stroke of a SMA-based system can be improved by up to 69.81% by using the tube-guided SMA wire actuator concept, which demonstrated the efficacy of the tube-guided SMA wire actuator concept [23]. In addition, they showed that graphite powder and tungsten disulfide lubricant both delivered better improvements in stroke [23]. Copaci *et al.* proposed different kinds of configurations of SMA-based actuator, such as the multiple SMA wires actuator, double actuator configuration, etc. These configurations are designed to investigate influences of types of SMA wires, materials of the Bowden cable sheath, multiple SMA wires on the performances (e.g. work frequency, electrical consumption, total movement length) of SMA-based actuators [24]. Nizamani *et al.* conducted research on novel cooling techniques to decrease the cycle time of the SMA. In their study, oil and grease are used as two kinds of coolant, which are sealed inside PTFE tubes to help cool down the SMA temperature before testing. It was found that the grease cooling reduced the cooling time up to 30% and oil cooling by 20% [25]. However, current research on tube-guided SMA actuators has not explained the relationships between parameters like the actuation force and stroke.

This paper proposes a phenomenological model of the tube-guided SMA actuator to describe how the actuation stroke changes in relation to the applied stress and temperature. It can be used for predicting the end-state performance (between fully detwinned martensite and austenite) of tube-guided SMA actuators. The structure of this paper is arranged as follows. Section 2 describes materials and testing methods, whereas in Section 3 the test results are analysed. Then, we propose a model of the tube-guided SMA actuator in Section 4, taking thermal expansion and creep effects into account. To verify the model, results of a series of tube-guided SMA actuator force-control tests are used to compare with the model predictions in Section 5.

## 2. Materials and methods

In the first set of experiments, the shape memory alloy wire and tube were separately tested to obtain their basic material properties. Subsequently, a series of validation experiments was performed on the tube-guided SMA actuator. A Dynamic Mechanical Analyser (DMA) Q800® of TA instruments was used for all tests.

### 2.1. Shape memory alloy wire

0.15 mm diameter FLEXINOL® SMA wires purchased from Dynalloy, Inc. were used in experiments. The alloy consists of nickel and titanium atoms in a ratio of exactly 50%/50% and has a listed activation temperature of 90 ℃ [3]. To allow for repeated cycling without degradation, it is suggested that stress applied

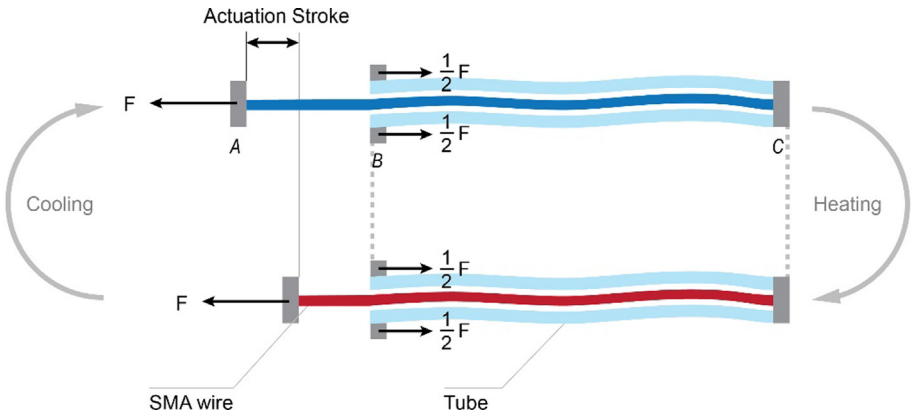


**Fig. 1.** Configuration and activation process of the tube-guided SMA actuator. The actuation is between points *A* and *B*, whereas most of the actuator length is in the flexible tail *BC*.

on the wire should be no more than 230 MPa at high temperature [3]. Four types of characterisation experiments were conducted.

(1) **Transformation Stress Tests:** The first experiment aims to figure out the martensite start transformation stress, martensite finish transformation stress, and their corresponding strain values. The Force-control condition was selected in the DMA testing program. During the tests, the SMA wire was loaded to 2.0 N (113 MPa) with a rate of 0.3 N/min, and then unloaded to 0.001 N with the same rate at room temperature (25 ℃).
(2) **SMA Young's Modulus Test:** The second experiment is to find out how the Young's modulus of the SMA wire changes with temperature. The strain controlled dynamic measurement module was used for the experiment. The testing temperature was programmed to increase from 30 ℃ to 160 ℃ with a rate of 1 ℃/min. In the program settings, we applied 15 μm displacement amplitude, 120% Force track and 1 Hz Frequency.
(3) **Transformation Temperatures Test:** In this test, the transformation temperatures are determined by heating and cooling specimens after uniaxial pre-straining in the martensite state [26]. The SMA wire was loaded with 2.0 N and heated to 120 ℃ with a rate of 10 ℃/min, followed by a 5 min isothermal soaking, and then it was cooled down to room temperature.
(4) **Force-control Tests:** In this series of experiments, the SMA wire was loaded with constant force (0 to 2.0 N with 0.1 N intervals) at room temperature. Then, it was heated to 120 ℃ with a rate of 10 ℃/min. After isothermal soaking for 5 min, the wire was cooled down to room temperature again. Strain values at 120 ℃ and 25 ℃, as well as the SMA actuation strain generated by the heating and cooling process can be approximated in each force-control test. A similar way of testing has been reported by Eschen *et al.* [7,27].

### 2.2. Tube

A Polytetrafluoroethylene (PTFE/teflon) tube (outer diameter 0.9 mm, inner diameter 0.4 mm) was selected for the tube-guided SMA actuator because of its low friction. The deformation of the tube consists of a thermal expansion (reversible) and a creep (non-reversible) contribution, the latter of which is a function of temperature, applied stress and time. The following five types of experiments on the tube were planned to characterize and model these contributions.

(1) **Thermal Expansion Tests:** A tube specimen with clamping length of 11.0 mm was heated from 25 °C to 160 °C with a rate of 5 °C/min under a constant force of 0.01 N. In order to correct for the thermal expansion of the clamping configuration, a calibration test with a quartz specimen was performed.
(2) **Tube Young's Modulus Test:** The Displacement Ramp method was selected in the DMA program. The displacement of the tube specimen increased from 0 to 3.0 mm with a rate of 0.5 mm/min at room temperature.
(3) **Preliminary Tests for Onset of Non-linear Creep:** A series of 5 min creep tests were conducted with a range of forces (0 to 2.0 N at 0.2 N intervals, 3.0 N, 4.0 N) at a constant temperature of 120 °C. The testing time was chosen to be of the same order as a typical actuation time in practical applications. Creep compliances of different forces at the fifth minute were recorded and compared. The sample lengths are again close to 11.0 mm. The tests are to identify the force range which would cause non-linear creep.
(4) **Time-Temperature Superposition Tests:** The forth series of experiments aims to figure out the influences of time and temperature on creep compliance. It is known that for most polymeric materials, superposition is obtained when shifting creep curves at different temperatures along the time axis. The overlapping curves form a so-called "master curve" [28]. By plotting the shift factor versus temperature, a shift factor curve can be obtained. The shift factor curve and the master curve form a convenient way of modelling the creep compliance as a function of temperature and time. For this Time-Temperature Superposition (TTS) testing we performed 10 min creep tests with 1.0 N force at temperatures between 30 °C and 120 °C. An isothermal soaking period of 5 min preceded the creep measurements. The temperatures were increased with 10 °C increments.
(5) **Effect of Temperature Cycling on Creep:** this experiment evaluates the effect of cyclic temperature change on the tube creep. A constant force of 1.0 N was applied to the tube after which the temperature was increased from 25 °C to 120 °C with a rate of 10 °C/min, kept isothermally for 15 min and then cooled down to 25 °C with the same rate. The heating-isothermal-cooling procedure was repeated three times.

### 2.3. Tube-guided SMA actuator

To determine the thermal–mechanical behaviour of the full tube actuator system in a more typical configuration, a tube length

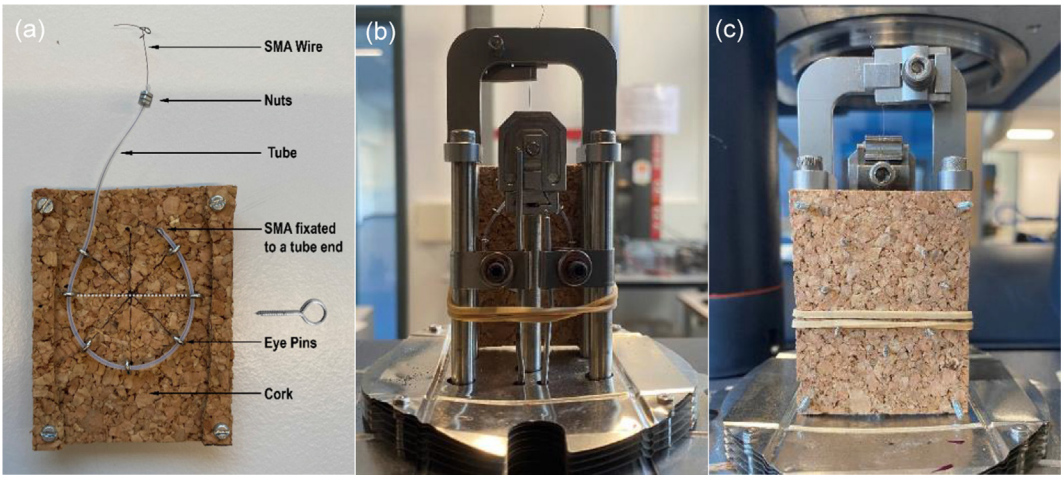


**Fig. 2.** (a) Setting of the tube-guided SMA actuator. (b) Back view of the experimental set-up. (c) Front view of the experimental set-up showing how the system is placed into the DMA machine.

of 114.5 mm was chosen. In order to be able to fit inside the oven of the Q800 instrument, the tube with SMA wire was fixated to a cork substrate in a circular shape (see Fig. 2(a)). The nut fixed at one end of the tube was clamped directly in the lower fixture of the DMA. The free SMA wire end was tied as a knot and inserted in the upper clamp. The experimental setup can be seen in Fig. 2(b) and (c). The entire tube-guided SMA actuator was fastened on the metal frame of the DMA machine with a rubber band.

To figure out how the displacement of the system changes under a constant force, the tube-guided SMA actuator was heated and cooled (from 25 °C to 120 °C) for three cycles with a rate of 5 °C/min under a constant force. Considering that the cork can delay the temperature change, a slower heating rate was selected for these system tests.

## 3. Characterisation results

### 3.1. Shape memory alloy wire

(1) **Transformation Stress Test (at room temperature):** As shown in Fig. 3, the stress–strain curve shows a first rapid elastic response followed by a second region with a much slower stress increase and a steeper upturn. The second region is attributed to the martensite to austenite transformation plateau. This room temperature stress–strain behaviour is modelled as three separate linear regions to get transformation stress and strain values, following the work of Rao [2].

The slope of $line_1$ can be interpreted as the Young's modulus of the twinned martensite SMA at room temperature. As for the $line_2$, it is suggested to be modelled as a horizontal line by using the stress level corresponding to 2.5% strain [2]. However, there is an obvious upward trend of the detwinning plateau in our test, so we decided to model this as a line with non-zero slope. For this, we drew three tangent lines for corresponding regions and got the values of the intersection points. The fitting parameters related to the start and finishing of the martensite transition are denoted as $\sigma_S^M$, $\sigma_F^M$ and $\varepsilon_F^M$, and the strain values at the 2.0 N end point as $\varepsilon_{2N}^M$. The values can be found in Table 1.

(2) **SMA Young's Modulus Test:** According to the testing results (Fig. S1 in the Supplement Information), the Young's Modulus of twinned martensite at room temperature is 24.4 GPa, which is very close to the slope of $line_1$ (25.7 GPa) in Fig. 3. The modulus of austenite at 120 ℃ is 40.5 GPa. The two values should be compared to values reported in literature, e.g. 28 GPa (martensite) and 83 GPa (austenite) [2]. More details can be found in Supplement Information.

(3) **Transformation Temperatures Test:** As depicted in Fig. 4, in the heating process, the strain remains at an almost constant level of 4.8% until the austenite start temperature ($A_s$). During the martensite to austenite phase transformation, the wire shrinks until the temperature reaches point $A_f$ (austenite finish temperature). In the subsequent cooling stage, we first observe a small strain increase due to thermal expan-

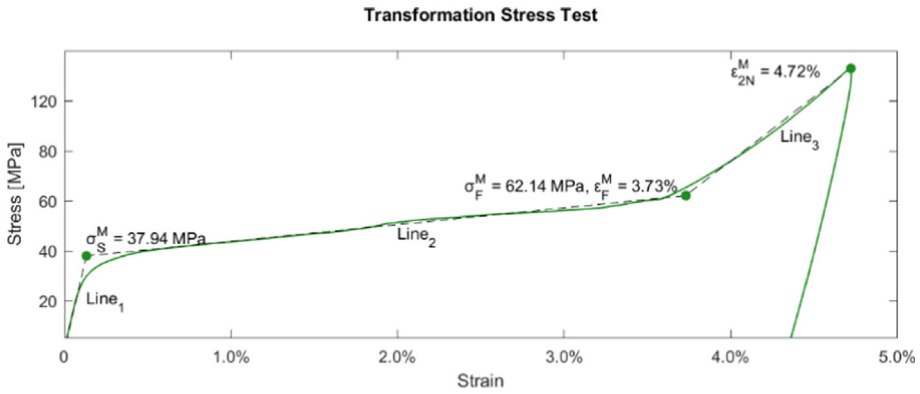


**Fig. 3.** Transformation stress and corresponding strains of the SMA wire at room temperature. Three grey dashed lines are tangent lines obtained from the experimental data.

**Table 1**
Properties of the FLEXINOL® SMA wire as determined in the experiments.

| Parameters of the FLEXINOL® Actuator Wire from DYNALLOY, Inc. | | |
|---|---|---|
| Martensite start transformation stress | $\sigma_S^M$ | 37.9 MPa |
| Martensite finish transformation stress | $\sigma_F^M$ | 62.1 MPa |
| Strain value of the martensite SMA wire under $\sigma_F^M$ | $\varepsilon_F^M$ | 3.73% |
| Strain value of the martensite SMA wire under $\sigma_{2N}$ | $\varepsilon_{2N}^M$ | 4.72% |
| Young's Modulus of austenite at 120℃ | $E_A$ | 40.5 GPa |
| Young's Modulus of twinned martensite at 30℃ | $E_M$ | 24.2 GPa |
| Austenite start temperature | $A_s$ | 84 ℃ |
| Austenite finish temperature | $A_f$ | 118 ℃ |
| Martensite start temperature | $M_s$ | 49 ℃ |
| Martensite finish temperature | $M_f$ | 42 ℃ |

sion, which is followed by a sudden larger expansion attributed to the martensite to austenite transformation ($M_s$ to $M_f$). The transformation temperature points$A_s$,$A_f$,$M_s$, and $M_f$ are obtained by plotting tangent lines to the experimental curves.

(4) **Force-control Tests:** The strain values after room temperature loading corresponding to specified load values are referred to as the martensite strain (blue triangles in Fig. 5). For stresses below 50 MPa, these strain values remain below 1%, but above the 50 MPa, much larger deformations are observed, which are attributed to the stress induced martensite to austenite transformation. Upon heating of these pre-stretched wires, they contract back to a strain value close to 0 (defined as the austenite strain, red open triangles in Fig. 5). The difference between the pre-stretch and recovery strain is the SMA actuation strain that SMA wire can generate. It is shown separately in Fig. 6.

The experimental results of the SMA wire are summarized in Table 1.

### 3.2. Tube

(1) **Thermal Expansion Test:** The coefficient of thermal expansion of the tube is determined as $1.31 \times 10^{-4}$ ℃$^{-1}$. More details can be seen in Fig. 2S of the Supplement Information.

(2) **Tube Young's Modulus Test:** The Young's modulus of the tube at room temperature is determined as 533 MPa, which compares well with the value of 410 MPa established by Brown under slightly different test conditions [29]. The graph of the Young's modulus also can be found in the Supplement Information.

(3) **Preliminary Tests for Onset of Non-linear Creep:** To figure out the creep properties of the tube we first established the onset of the non-linearity. A series of 5 min creep tests with increasing force at a chosen temperature (120 ℃) was performed. The non-linearity is assumed to start as soon as the ratio between measured creep and applied force (i.e. the creep compliance) starts to deviate from its initial value. Based on Fig. 7, we determined the linear creep range of the Teflon tube material to be between 0 and 2.0 N. Since the non-linear behaviour increases with rising temperature, the 0–2.0 N range is also expected to be valid for temperatures below 120 ℃.

(4) **Time-Temperature Superposition Test:** Based on the above findings the creep tests were performed with a force of 1.0 N, and the resulting compliance curves between 0 and 10 min are shown in Fig. 8 as the coloured lines. In polymer engineering it is customary to shift the creep curves obtained at different temperatures along the time axis to form a so-called master curve and determining the corresponding shift factor. This has the advantage that in this way only models for two experimental curves are needed to predict creep data within a large time and temperature range. For a more detailed explanation we refer to e.g. Ferry's research [28]. The grey line in Fig. 8 is the above-mentioned master curve and the shift factor $a_T(T)$ is shown in the inset.

(5) **Effect of Temperature Cycling on Creep:** In this test, the influence of temperature cycles as used in the validation experiments on thermal expansion and creep is evaluated. Changes of temperature and strain during the experiment are plotted as red and blue accordingly in Fig. 9. A single cycle consists of an 11 min heating period, a 15 min isothermal period and a cooling period of about 15 min. It can be seen that the strain shows a large increase (5.24%) during the first heating cycle and follows a more cyclic behaviour in subsequent cooling and heating cycles. The cyclic strains of the second and third cycles reflect the thermal contraction and expansion of the tube.

As seen in Fig. 9 for the second cycle (40–80 min), the changes in strain during heating and cooling are 1.24% and 1.26% respectively, which are very close to the strain value 1.24% as calculated from the coefficient of thermal expansion in combination with a temperature difference of 95 ℃. The total strain change over the 2nd cycle is about 0.27%, which is of the same magnitude as the creep strain (0.28%) during the 120 ℃ holding time.

## 4. Modelling

### 4.1. Mechanical model

The actuation stroke of the system in Fig. 1 depends on the actuation strain of the SMA wire and the compression strain of the tube. Both strain contributions are modelled as described in Eqs. (1) and (2) below. As shown in Fig. 6, the SMA actuation strain versus stress curve can be modelled as 3 linear parts:.

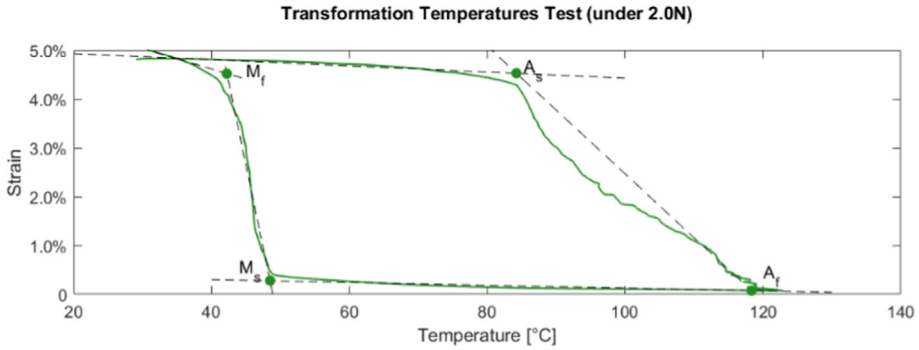


**Fig. 4.** Transformation temperature diagram of the SMA wire (testing range: 20–120 ℃).

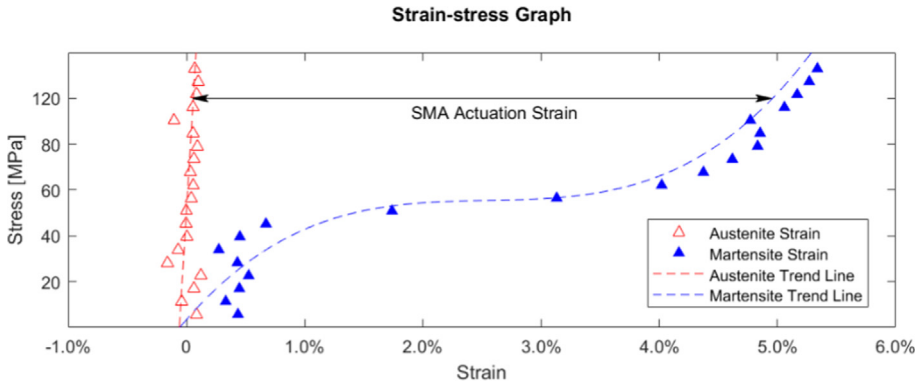


**Fig. 5.** Strain values at 120 ℃ and 25 ℃ for different applied stress levels. Blue triangles: strain values after pre-stretching at 25 ℃; Red open triangles: recovery strain values after heating to 120 ℃. The blue dashed line is a 3rd degree polynomial trend line fitted to the martensite data, and the red dashed line is a linear line fitted to the austenite data. (For interpretation of the references to colour in this figure legend, the reader is referred to the web version of this article.)

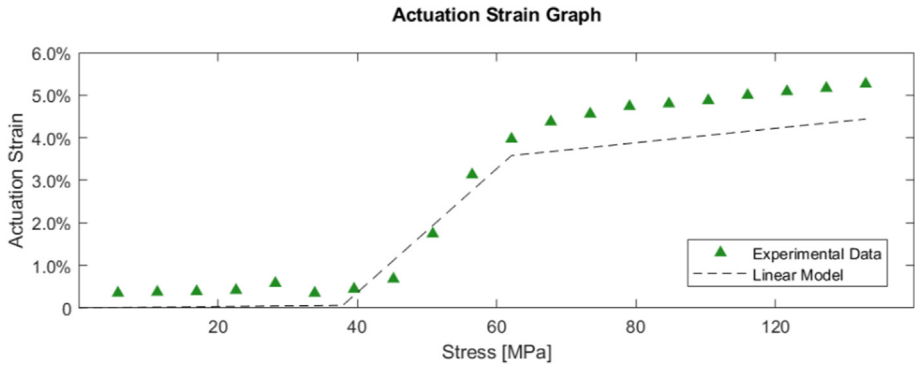


**Fig. 6.** Actuation strain values under different constant stresses. The dashed line is based on Figs. 3 and 5, and fitted to Eq.(1).

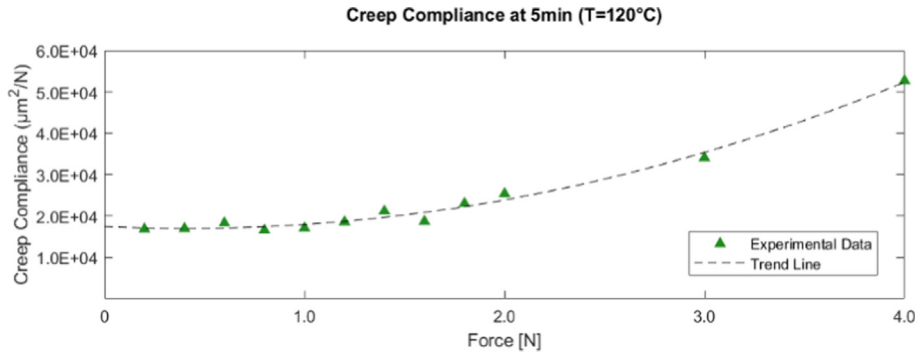


**Fig. 7.** Creep compliance under different forces at the fifth minute (T = 120 °C). The dashed line is a 2nd degree polynomial trend line fitted to the experimental data.

$$\Delta\varepsilon_M^{SMA} = a_i + b_i\sigma^{SMA} \tag{1}$$

where $\Delta\varepsilon_M^{SMA}$ is the actuation strain of the SMA wire, $\sigma^{SMA}$ is the applied stress to the SMA wire, $a_i$ and $b_i$ are the constants corresponding to the 3 different parts ($i$ = 1, 2, 3). As an alternative, a more detailed model is presented in Supplement Information.

The compression of the tube is given as:.

$$\Delta\varepsilon_M^{tube} = \frac{\sigma^{tube}}{E^{tube}} = \sigma^{tube}D^{tube} \tag{2}$$

where $\Delta\varepsilon_M^{tube}$ is the compression strain of the tube and $E^{tube}$ is the Young's modulus of the tube, $\sigma^{tube}$ is the applied stress to the tube, $D^{tube}$ is the creep compliance.

With the Eqs. (1) and (2), the actuation stroke of the tube-guided SMA actuator,$S_M$, becomes:.

$$S_M = S_M^{SMA} + S_M^{tube} = \Delta\varepsilon_M^{SMA}l^{SMA} + \Delta\varepsilon_M^{tube}l^{tube} \tag{3}$$

in which $l^{SMA}$ and $l^{tube}$ denote the lengths of the SMA wire and tube parts, respectively.

A series of pre-tests show that friction has little influence on the actuation stroke, so it is omitted in the model.

### 4.2. Correction for thermal expansion

In addition, the thermal expansion differences between tube and SMA wire has influence on the stroke of the tube-guided SMA actuator:.

$$S_T = S_T^{SMA} - S_T^{tube} = (\alpha^{SMA}l^{SMA} - \alpha^{tube}l^{tube})\Delta T \tag{4}$$

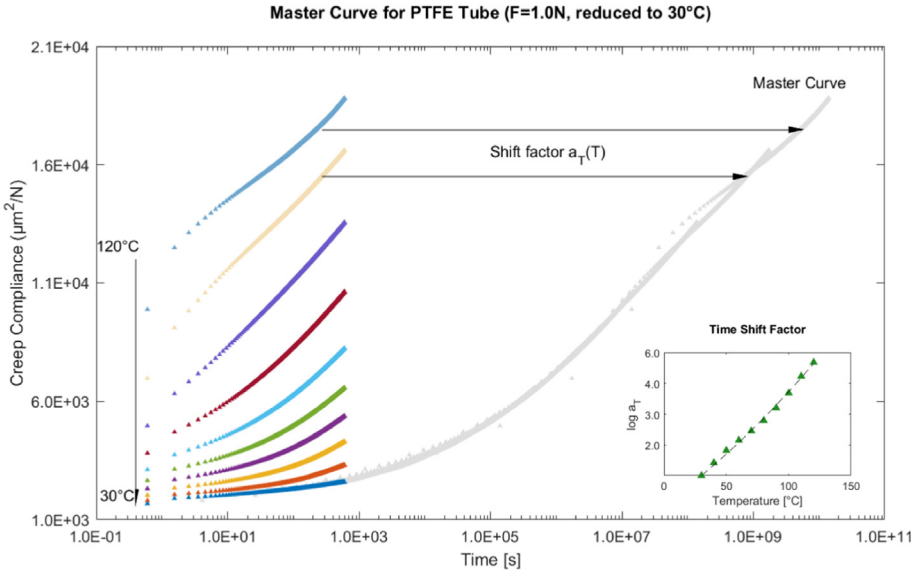


**Fig. 8.** The master curve and shift factor for the tube (F = 1.0 N, reduced temperature set at 30 °C).

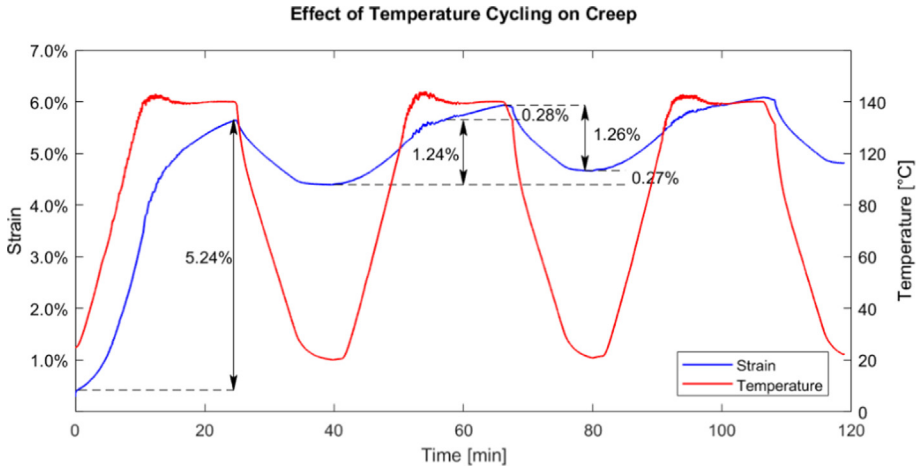


**Fig. 9.** The effect of temperature cycling on tube creep (under a constant force of 1.0 N). Blue line is strain, red line is temperature. (For interpretation of the references to colour in this figure legend, the reader is referred to the web version of this article.)

where $S_T$ is the thermal expansion displacement of the system, $\alpha^{SMA}$ is the coefficient of thermal expansion of the SMA wire, $\alpha^{tube}$ is the coefficient of thermal expansion of the tube, and $\Delta T$ is the change of temperature.

### 4.3. Correction for creep

As for the creep, a Cross function is adopted to describe the measured creep compliance master curve:.

$$D = D_g + \frac{D_r}{1 + (t_{red}/\tau)^{-m}} \tag{5}$$

where $D_g$ is the glassy compliance, $D_r$ is the rubbery compliance, $\tau$ and $m$ are parameters and $t_{red}$ is the so-called reduced time which is defined as [28]:.

$$t_{red} = \int_0^t a_T dt \tag{6}$$

where $t$ is the real time and $a_T$ is the temperature shift factor.

Note that for a constant temperature, the reduced time reads as $t_{red} = a_T t$ which can be understood as that at a certain temperature, say 50 ℃, the creep proceeds a factor $a_T$ faster than at the reference temperature. In our case (see Fig. 8) the shift factor at 50 ℃ is $10^2$ so creep at that temperature is 100 times faster than at 30 ℃. The integral in Eq. (6) is only needed for non-isothermal processes [28].

Several models have been proposed for approximating the shift factor$a_T$, such as the Williams-Landl-Ferry and the Arrhenius equation [30,31]. Here a second order polynomial for $log a_T$ was considered more convenient to describe the measured data:.

$$log a_T = c_1(T - T_r) + c_2(T - T_r)^2 \tag{7}$$

where $c_1$ and $c_2$ are constants, $T_r$ is the chosen reference temperature and $T$ is the temperature.

When taking creep into account the mechanical tube strain in Eq. (2),$\varepsilon^{tube} = \sigma^{tube} D^{tube}$, is replaced with the time and temperature dependent compliance:$\varepsilon^{tube} = \sigma^{tube} D^{tube}(T,t)$. The creep displacement part,$S_C$, then becomes:.

$$S_C = \sigma^{tube} D(T,t) l^{tube} \tag{8}$$

### 4.4. Modelling of the tube-guided SMA actuator

The aim of the phenomenological model of the tube-guided SMA actuator is to predict how the actuation stroke of the system

changes during heating and cooling under a constant force. Although the stress of the SMA wire and the tube are not the same owing to their different cross-sectional areas, the $\sigma^{SMA}$ and $\sigma^{tube}$ can be obtained easily with the formula$\sigma = F/A$. Hence, the stress $\sigma^{SMA}$ and $\sigma^{tube}$ are selected as input values and the system actuation stroke $S$ is the output value of the model. The overall stroke can be considered as the sum of the actuation of the SMA wire, compression, thermal expansion and creep of the tube:.

$$S(\sigma^{SMA}, \sigma^{tube}, T, t) = S_M(\sigma^{SMA}, \sigma^{tube}) + S_T(T) + S_C(\sigma^{tube}, T, t) \quad (9)$$

where $S(\sigma^{SMA}, \sigma^{tube}, T, t)$ is the actuation stroke of the tube-guided SMA actuator in a loading/heating/cooling stage.

(1) **Loading Stage:** The strain change of the SMA wire during loading is shown as a blue curve in Fig. 5. To make the model more general for different stages, we still use the Eq. (1) to calculate the SMA actuation strain at this stage. As for the tube, if the loading is at room temperature, the tube displacement can either be obtained from Eq. (2) or, alternatively, from Eqs. (5) and (8) with$D = D_g$. The $S_T$ and $S_C$ are not considered at this stage.

(2) **Heating Stage:** During the heating process, both the $S_M^{SMA}$ and $S_T$ are negative, because actuation of the SMA wire and the thermal expansion of the tube would result in a shortening of the distance *AB* in Fig. 1. The coefficient of thermal expansion of the SMA which varies between 6.6 and 11 $\times$ $10^{-6}$ ℃$^{-1}$ [2] is much smaller than that of the tube (1.31 $\times$ $10^{-4}$ ℃$^{-1}$, Thermal Expansion Test in the Supplement Information). We therefore omit the thermal expansion of the SMA wire in our model. The creep of the tube is the largest during the first heating stage and leads to extra tube compression, resulting in a positive $S_C$ contribution and a larger stroke.

(3) **Cooling Stage:** Both the $S_M^{SMA}$ and $S_T$ are positive in this stage. As discussed in section 3.2, there is little creep during the cooling process. Therefore, the $S_C$ can be neglected during cooling.

## 5. Validation and discussion

### 5.1. Parameters fitting of the model

With the material parameters listed in Table 1 and Equations (1)-(9), the $a_i$ and $b_i$ parameters for the SMA stroke model were calculated and presented in Table 2.

For the creep model of the tube material, the master curve and shift factor parameters as well as their error bounds were determined by using a Matlab fitting procedure. The parameters of Equation (11) and (13) are listed in Table 3.

### 5.2. Validation

Here we consider the performance of the complete actuator system during a series of three heating and cooling cycles similar to the Teflon tube experiments of Fig. 9. As depicted in Fig. 10, the actuation stroke shows regular changes with temperature except for the first heating period of the system. To facilitate the discussion, we define four different zones (I - IV, see Fig. 10).

(1) **Zone I:** The tube-guided SMA actuator is loaded with a constant force in the first few minutes. During the loading process, the SMA wire is stretched and transforms to the detwinned martensite phase whereas at the same time the tube is compressed. These lead to the displacement increase $\Delta S_1$ in the Zone I.

**Table 2**
Parameters for the SMA wire model.

| $a_1$ | $b_1$ [%/MPa] | $a_2$ [%] | $b_2$ [%/MPa] | $a_3$ [%] | $b_3$ [%/MPa] |
|---|---|---|---|---|---|
| 0 | 0.0017 | −5.4430 | 0.1451 | 2.5200 | 0.0170 |

**Table 3**
Parameters for the tube model.

| $D_r$[MPa$^{-1}$] | $D_g$[MPa$^{-1}$] | $\tau$[s] | $m$ | $T_r$[°C] | $c_1$ | $c_2$ |
|---|---|---|---|---|---|---|
| 2.05 $\times$ $10^4$ (±280) | 1600 (±50) | 4.01 $\times$ $10^7$ (±0.4 $\times$ $10^7$) | 0.259 (±4.4 $\times$ $10^{-3}$) | 30 | 6.69 $\times$ $10^{-2}$ (±0.8 $\times$ $10^{-2}$) | 1.6 $\times$ $10^{-4}$ (±1 $\times$ $10^{-4}$) |

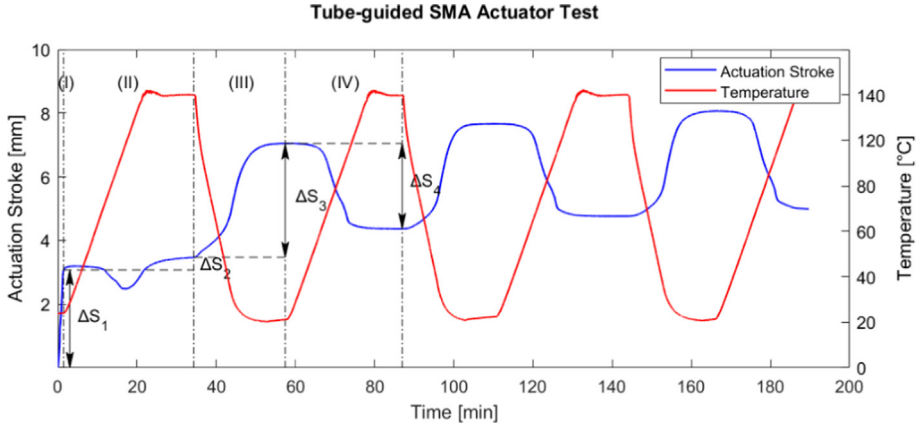


**Fig. 10.** Analysis of the tube-guided SMA actuator test. Blue line is the actuation stroke; red line is the temperature.$\Delta S_1$: the displacement of the loading stage;$\Delta S_2$: the displacement of the first heating stage;$\Delta S_3$: the displacement of the cooling stage;$\Delta S_4$: the displacement of the second heating stage. (For interpretation of the references to colour in this figure legend, the reader is referred to the web version of this article.)

(2) **Zone II:** The tube-guided SMA actuator is heated to 120 °C at a rate of 5 °C/min and isothermally kept for 15 min. At the beginning, creep and thermal expansion of the tube almost counteract with each other, so there is little change of the displacement. With the temperature increase, the SMA reaches its austenite start temperature, and leads to contraction. It explains why the displacement of the system decreases after the initial plateau. However, the creep of the tube always results in an increase in the displacement of the system. When contraction of the SMA is less than the expansion caused by creep of the tube, displacement of the system increases again. In the isothermal environment of 120 °C, the displacement rises slightly owing to the creep of the tube. Overall, the displacement of the actuator system during the first heating ($\Delta S_2$) is very different from that of the following temperature cycles.

(3) **Zone III:** The system is cooled down to 25 °C and kept at this temperature for 15 min, the SMA wire transforms from the austenite state to the detwinned martensite state, which leads to an expansion of the system under a constant force. Its increase in length results in a larger displacement of the actuator system. As for the tube, the creep contributes to the displacement increase. However, in comparison with the previous process, the creep has much less influence on the displacement. Cooling contraction of the tube also leads to an increase of the system's displacement$\Delta S_3$.

(4) **Zone IV:** The tube-guided SMA actuator is heated to 120 °C and kept isothermally for 15 min again. In this process, the shape memory effect of the SMA wire and thermal expansion of the tube lead to a decrease of the displacement$\Delta S_4$.

A more detailed analysis can be found in Model Simulation of the Supplement Information, in which we can see how displacements of SMA actuation, thermal expansion and creep of the tube change in different stages.

In addition, it should be noted that all experiments were performed under controlled heating and cooling conditions which minimizes possible thermal gradients in the actuator. The actuator can also be activated by Joule heating outside the oven. In that case the actuation cycle is in the order of seconds/ minutes, which is much faster than it shows in Fig. 10.

### 5.3. Discussion

The displacements$\Delta S_1$,$\Delta S_2$, $\Delta S_3$ and $\Delta S_4$ as indicated in Fig. 10 are recorded for each force setting (0 to 1.6 N at 0.2 N intervals) and compared with the theoretical results of the model. The results are shown in Fig. 11.

Fig. 11(a) shows the measured (dashed green line) and calculated (full green line) loading displacements during the loading stage$\Delta S_1$, as well as the corresponding results for the first heating stage, $\Delta S_2$ (yellow lines). In both cases, the predicted values agree

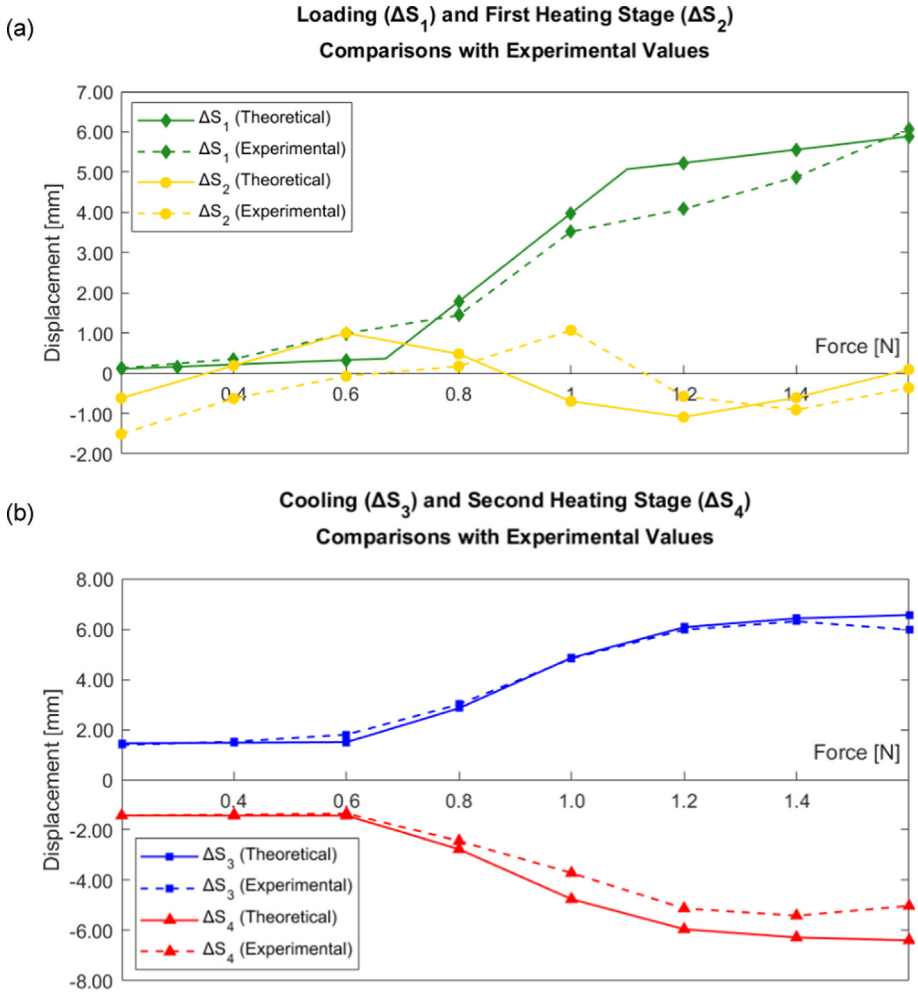


**Fig. 11.** Comparisons between the theoretical (full lines) and experimental (dashed lines) results. The $\Delta S_i$ refers to Fig. 10.

well with the measured stroke displacements (differences are about 1 mm or less) and the trend of an increasing stroke above 0.8 N for $\Delta S_1$ is well captured.

In addition, Fig. 11(b) shows that also the stroke displacement during cooling,$\Delta S_3$, and during the second heating stage, $\Delta S_4$ are well captured by the model.

In the following content, we discuss the measured and predicted actuator displacements during the four different stages in more detail.

(1) Loading Stage, $\Delta \boldsymbol{S}_1$

With Fig. 11(a), the experimentally observed displacement $\Delta S_1$ of the loading process agrees well with the theoretical results. Smaller deviations can be observed for forces above 0.8 N. There are two possible explanations for this. First, if the SMA wire is not fully stretched (especially the exposed part, *AB* in Fig. 1), or there is an initial sliding between the tube-guide SMA actuator and the clamp, it can lead to larger displacement values. Second, even though the actuator is preconditioned by heating to 120 ℃ under a constant low force before each test, it is still difficult to ensure the SMA is initially at the fully twinned martensite phase, which may lead to lower displacement values.

(2) First Heating Stage, $\Delta \boldsymbol{S}_2$

During the loading step, the tube part is compressed but shows only a small compression displacement due to its relatively high modulus ($E^{tube}$ = 533 MPa). When it is heated, two things occur in the tube. First, the tube starts to expand due to thermal expansion effects, leading to a decrease of the actuation stroke. Next to that, the material rapidly becomes softer at higher temperature and creep becomes noticeable. The creep effects are described by Eq. (8) and result in an increased actuation stroke. As for the SMA wire, the temperature driven conversion to the austenite phase leads to a contraction contribution. The combination of thermal expansion, creep and SMA actuation during the first heating period results in a stroke displacement decrease followed by a rapid increase, as observed in Zone II of Fig. 10. Since all effects almost balance out, the net displacements during the first heating stages are close to zero. An effect which is well captured by our model predictions for $\Delta S_2$ (see Fig. 11(a)). A more detailed analysis can be seen in the Model Simulation of the Supplement Information.

(3) Cooling Stage, $\Delta \boldsymbol{S}_3$

As depicted in Fig. 11(b), the experimental results for $\Delta S_3$ (blue dashed line) fit well with the theoretical results (full blue line). During cooling additional creep effects are small and the stroke displacement is mainly determined by the SMA phase transformation strains plus the thermal expansion of the tube. The good agreement between observations and predictions here indicate that those two contributions are well modelled.

(4) Second Heating, $\Delta \boldsymbol{S}_4$

The second (and subsequent) heating stages under constant loading differ from the first heating period in their creep contributions. As explained before, during the first heating the creep which does not yet occur at room temperature sets in, resulting in a large first creep displacement effect. However, since the load is kept on the sample, all subsequent cooling and heating periods only result in a slowing down or acceleration of the *reduced* creep time but not to creep recovery. The first large creep effect is thus not repeated and the next temperature cycles are just subsequent parts on *the same creep curve*. In order to illustrate this more clearly we replot the creep data at 120 °C and corresponding prediction on a linear time scale in Fig. 12, and indicate the large differences in creep contributions during the first and the second heating cycles.

The deviation between the experimental and modelled results ($\Delta S_4$) increases with higher force, which is larger than the difference in the cooling process. In Section 3.2, even though we determine the linear creep range of the tube to be 0–2.0 N, there shows a slight upward trend above about 1.0 N, which means that the actual creep compliance above 1.0 N could be slightly larger than the calculated value in our model, which explains the deviation between the theoretical and experimental results after 0.8 N to some extent. In general, the predicted values also fit well with the experimental data.

## 6. Conclusion and outlook

A phenomenological model of tube-guided SMA actuators is proposed in this article. For the cooling and second heating stage (blue and red curves in Fig. 11), the average deviation over the full force range (0.2–1.6 N) between modelled and test results is 9.6%, although the deviation (27.3%) is much larger at the maximum force (1.6 N of $\Delta S_4$). The model reveals the relationship between the actuation stroke and applied stresses with time and, temperature as independent variables. After determining the basic parameters of the SMA wire (e.g. transition temperatures, diameters, Young's modulus of austenite and twinned martensite, transformation stress and corresponding strain), together with time–temperature dependence of the tube creep compliance, the actuation stroke of the entire system can be calculated for given input stress values. Creep of the Teflon tube is included in the model to show that, if needed, the model can fully capture the actuator behavior.

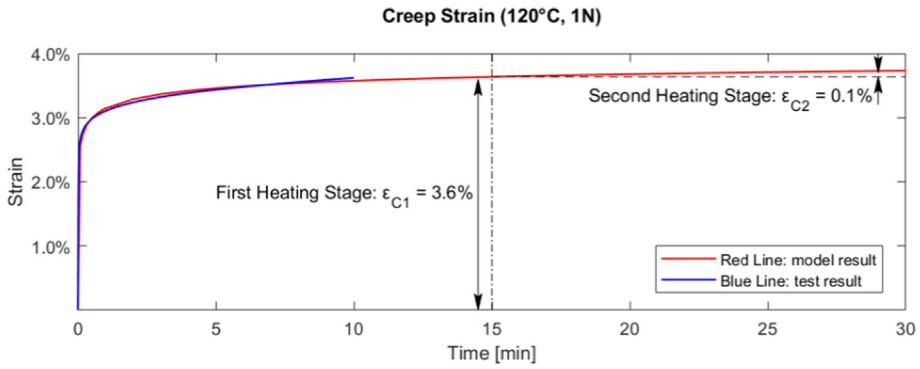


**Fig. 12.** The creep strain of the tube at 120 °C. The red curve is modelled in Matlab with Eqs. (5)-(7). The blue curve is the result of the third test in section 3.2. (For interpretation of the references to colour in this figure legend, the reader is referred to the web version of this article.)

Our results also indicate that for the second and next heating cycles under constant loading, the creep contribution is negligible. In that case, the actuator model can be simplified by neglecting the creep term. As an alternative, one could also choose to design the actuator with a tube material which exhibits less creep in the operating temperature range.

The model proposed in this research bridges the gap between the smart material science and practical design approach. It supports designers who are not specialized in the field of shape memory materials, to efficiently adopt the tube-guide SMA actuator system in their design without having to work with complicated constitutive material models.

Tube-guided SMA actuators are thin, flexible, light-weight, noiseless and still have a relatively large actuation stroke and force. They are particularly useful as actuators in applications where motors or other actuator types are not suited like in clothing or directly on the human skin. Tube-guided SMA actuators have promising prospects in the fields of wearable actuators and soft robotics. In the Supplement Information, examples are given of a skin-mounted haptic device and a smart insulation control garment, which could bring inspirations to designers and engineers at application levels.

## 7. Data availability

The data that support the findings of this research are available from the corresponding author upon reasonable request.

## CRediT authorship contribution statement

**Qiang Liu:** Conceptualization, Validation, Writing – original draft, Writing – review & editing. **Sepideh Ghodrat:** Conceptualization, Validation, Supervision, Writing – review & editing. **Kaspar M.B. Jansen:** Conceptualization, Supervision, Validation, Writing – review & editing.

## Declaration of Competing Interest

The authors declare that they have no known competing financial interests or personal relationships that could have appeared to influence the work reported in this paper.

## Acknowledgements

This research was supported by an internal funding from Delft University of Technology (TU Delft). The authors gratefully acknowledge financial support from China Scholarship Council (Grant No. 202006130029).

## Appendix A. Supplementary material

Supplementary data to this article can be found online at https://doi.org/10.1016/j.matdes.2022.110571.

## References

[1] M. Bengisu, M. Ferrara, Materials that move: smart materials, intelligent design, Springer, 2018.
[2] A. Rao, A.R. Srinivasa, J.N. Reddy, Design of shape memory alloy (SMA) actuators, Springer, 2015.
[3] DYNALLOY. "Technical Characteristics of FLEXINOL® Actuator Wires." https://www.dynalloy.com/pdfs/TCF1140.pdf (accessed 17-10, 2021).
[4] F. Cao, M. Y. Saraiji, and K. Minamizawa, "Skin+ programmable skin as a visuo-tactile interface," in *ACM SIGGRAPH 2018 Posters*, 2018, pp. 1-2.
[5] D. Hwang, J. Lee, K. Kim, On the design of a miniature haptic ring for cutaneous force feedback using shape memory alloy actuators, Smart Mater. Struct. 26 (10) (2017) 105002, https://doi.org/10.1088/1361-665X/aa860d.
[6] T. Nakao *et al.*, "ShareHaptics," presented at the ACM SIGGRAPH 2019 Posters, 2019.
[7] K. Eschen, R. Granberry, B. Holschuh, J. Abel, Amplifying and Leveraging Generated Force Upon Heating and Cooling in SMA Knitted Actuators, ACS Appl. Mater. Interfaces 12 (48) (2020) 54155–54167.
[8] J.C. Duvall, L.E. Dunne, N. Schleif, B. Holschuh, Active "hugging" vest for deep touch pressure therapy, presented at the Proceedings of the 2016 ACM International Joint Conference on Pervasive and Ubiquitous Computing: Adjunct, 2016.
[9] R. Sachdeva, S. Miyazaki, and Z. Dughaish, "Nitinol as a biomedical material," *Encyclopedia of materials: science and technology*, pp. 6155-6160, 2001.
[10] D. Stoeckel, Nitinol medical devices and implants, Minim. Invasive Ther. Allied Technol. 9 (2) (2000) 81–88.
[11] J. Mohd Jani, M. Leary, A. Subic, M.A. Gibson, A review of shape memory alloy research, applications and opportunities, Mater. Des. 1980–2015 (56) (2014) 1078–1113, https://doi.org/10.1016/j.matdes.2013.11.084.
[12] V. Antonucci, F. Auricchio, L. Lecce, E. Sacco, Shape Memory Alloy Engineering: For Aerospace, Structural, and Biomedical Applications, Butterworth-Heinemann, 2021.
[13] M. Balasubramanian, R. Srimath, L. Vignesh, and S. Rajesh, "Application of shape memory alloys in engineering–A review," in *Journal of Physics: Conference Series*, 2021, vol. 2054, no. 1: IOP Publishing, p. 012078.
[14] MarketsAndMarkets. "Key Revenue Pockets & Shape Memory Alloys Market Industry Leaders." http://www.marketsandmarketsblog.com/shape-memory-alloys-market.html (accessed 17-10, 2021).
[15] K. Tanaka, S. Nagaki, A thermomechanical description of materials with internal variables in the process of phase transitions, Ingenieur-Archiv 51 (5) (1982) 287–299.
[16] L.C. Brinson, A. Bekker, S. Hwang, Deformation of shape memory alloys due to thermo-induced transformation, Journal of intelligent material systems and structures 7 (1) (1996) 97–107.
[17] K. Ikuta, M. Tsukamoto, and S. Hirose, "Mathematical model and experimental verification of shape memory alloy for designing micro actuator," in *[1991] Proceedings. IEEE Micro Electro Mechanical Systems*, 1991: IEEE, pp. 103-108.
[18] S.-M. An, J. Ryu, M. Cho, K.-J. Cho, Engineering design framework for a shape memory alloy coil spring actuator using a static two-state model, Smart Mater. Struct. 21 (5) (2012) 055009.
[19] N. J. Ganesh, S. Maniprakash, L. Chandrasekaran, S. Srinivasan, and A. Srinivasa, "Design and development of a sun tracking mechanism using the direct SMA actuation," 2011.
[20] T. Veldhoen, Designing a Shape Shifting Object (2019).
[21] A. Villoslada, A. Flores, D. Copaci, D. Blanco, L. Moreno, High-displacement flexible shape memory alloy actuator for soft wearable robots, Rob. Auton. Syst. 73 (2015) 91–101.
[22] I. Galiana, F. L. Hammond, R. D. Howe, and M. B. Popovic, "Wearable soft robotic device for post-stroke shoulder rehabilitation: Identifying misalignments," in *2012 IEEE/RSJ International Conference on Intelligent Robots and Systems*, 2012: IEEE, pp. 317-322.
[23] T. Helps, A. Vivek, J. Rossiter, Characterization and Lubrication of Tube-Guided Shape-Memory Alloy Actuators for Smart Textiles, Robotics 8 (4) (2019) 94.
[24] D. Copaci, D. Blanco, and L. E. Moreno, "Flexible shape-memory alloy-based actuator: Mechanical design optimization according to application," in *Actuators*, 2019, vol. 8, no. 3: Multidisciplinary Digital Publishing Institute, p. 63.
[25] A. M. Nizamani, J. Daudpoto, and M. A. Nizamani, "Development of faster SMA actuators," *Shape memory alloys-fundamentals and applications,* pp. 106-126, 2017.
[26] Astm, Standard Test Method for Mechanical Uniaxial Pre-strain and Thermal Free Recovery of Shape Memory Alloys, ASTM Standard (2018).
[27] K. Eschen, R. Granberry, J. Abel, Guidelines on the design, characterization, and operation of shape memory alloy knitted actuators, Smart Mater. Struct. 29 (3) (2020) 035036.
[28] J.D. Ferry, Viscoelastic properties of polymers, John Wiley & Sons, 1980.
[29] R. Brown, Handbook of polymer testing: physical methods, CRC Press, 1999.
[30] M.L. Williams, R.F. Landel, J.D. Ferry, The temperature dependence of relaxation mechanisms in amorphous polymers and other glass-forming liquids, J. Am. Chem. Soc. 77 (14) (1955) 3701–3707.
[31] K.J. Laidler, The development of the Arrhenius equation, J. Chem. Educ. 61 (6) (1984) 494, https://doi.org/10.1021/ed061p494.